Investigation of Pyrolysis Products of Propylenimine by Gas Electron Diffraction Combined with *ab Initio* Calculations. Molecular Structures of $CH_3-NH-CH=CH_2$ and $CH_3-N=CH-CH_3$

Hideo Fujiwara, Toru Egawa, and Shigehiro Konaka*

Contribution from the Department of Chemistry, Faculty of Science, Hokkaido University, Sapporo 060, Japan

Received April 1, 1996[⊗]

Abstract: Pyrolysis products of propylenimine have been investigated by gas electron diffraction aided by mass spectrometry. Propylenimine vapor was heated in a quartz tube and effused into the diffraction chamber through a nozzle kept at room temperature. When the temperature of the quartz tube was 470 °C, propylenimine completely transformed into *syn*- and *anti*-$CH_3-NH-CH=CH_2$ (*N*-methylvinylamine) and *trans*-$CH_3-N=CH-CH_3$ (*N*-methylethylidenimine), all of which are short-lived species. Geometrical structures and mole fractions of these species were determined from electron diffraction data combined with the results of *ab initio* calculations. The principal structural parameters of *syn*-$CH_3-NH-CH=CH_2$ are as follows: $r_g(N-C_{vinyl}) = 1.391(3)$ Å; $r_g(N-C_{methyl}) = 1.465(3)$ Å; $r_g(C=C) = 1.343(4)$ Å; $\angle_\alpha CNC = 119.5(9)°$; $\angle_\alpha NCC = 126.5(7)°$. Those of *anti*-$CH_3-NH-CH=CH_2$ are as follows: $r_g(N-C_{vinyl}) = 1.395$ Å; $r_g(N-C_{methyl}) = 1.472$ Å ; $r_g(C=C) = 1.341$ Å; $\angle_\alpha CNC = 118.4°$; $\angle_\alpha NCC = 126.1°$. Those of *trans*-$CH_3-N=CH-CH_3$ are as follows: $r_g(N=C) = 1.278$ Å; $r_g(N-C) = 1.472$ Å; $r_g(C-C) = 1.511$ Å; $\angle_\alpha CNC = 118.0°$; $\angle_\alpha NCC = 121.4°$. Parenthesized values are the estimated limits of error (3σ) referring to the last significant digit. No error estimation is given for dependent parameters. The determined mole fractions of *syn*- and *anti*-NMVA and *trans*-NMEI are 0.63(7), 0.28(8), and 0.09(4), respectively. The experimental data of electron diffraction obtained at 530 °C could best be reproduced by partial inclusion (about 30%) of decomposition products such as ketenimine and methane. The reaction path has been discussed on the basis of the temperature dependence of the amount of the unstable species.

Introduction

The pyrolysis of propylenimine (PI, 2-methylaziridine) was first investigated by Günthard and co-workers.[1−3] They heated PI in a quartz tube using a gas phase flow system over 510 °C and detected *N*-methylethylidenimine (NMEI; $CH_3-N=CH-CH_3$) by IR, mass, and ^{1}H-NMR spectroscopy.[1] Later, the conformation of NMEI was determined to be *trans* by measuring microwave spectra of the normal and deutrated species (see Figure 1).[2] They also measured IR spectra in the gas phase and Ar matrix.[3]

About one decade ago, new knowledge of the pyrolysis reaction of PI was brought about by two groups almost simultaneously.[4,5] Amatatsu et al.[4] measured the IR spectrum of the products of the reaction system similar to those in refs 1 and 2. They revealed that a transient species, *N*-methylvinylamine (NMVA; $CH_3-NH-CH=CH_2$), formed at first and then it turned into *trans*-NMEI. NMVA is expected to have two stable conformers, *syn* and *anti*, as shown in Figure 1 (They were called *cis* and *trans*, respectively, in refs 4 and 5). However, they could not determine whether only one conformer or both appeared on their spectrum and they assumed that only *syn* conformer existed on the basis of *ab initio* calculations. On the other hand, Sugie et al. measured the microwave spectrum of the same pyrolysis system and assigned the observed spectral lines to the rotational transitions of *syn*-NMVA and *trans*-

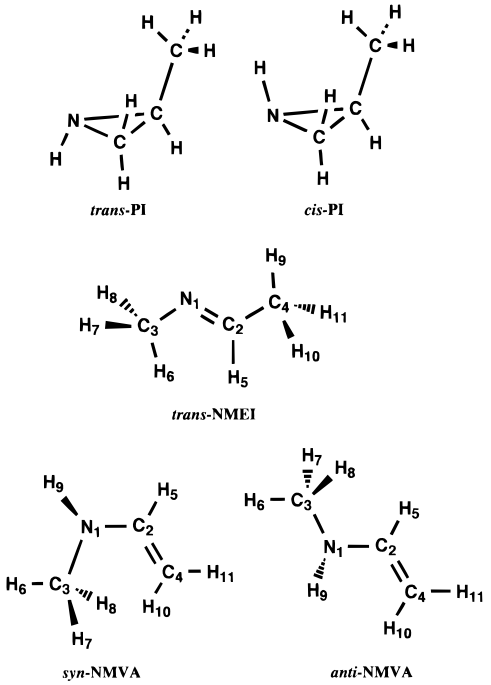

Figure 1. Molecular models for *trans*- and *cis*-propylenimine (PI), *trans*-*N*-methylethylidenimine (NMEI), and *syn*- and *anti*-*N*-methylvinylamine (NMVA) with atom numbering.

* Address correspondence to this author.

⊗ Abstract published in *Advance ACS Abstracts,* January 15, 1997.

(1) Meier, J.; Akermann, F.; Günthard, Hs. H. *Helv. Chim. Acta* **1968**, *51*, 1686−1691.
(2) Meier, J.; Bauder, A.; Günthard, Hs. H. *J. Chem. Phys.* **1972**, *57*, 1219−1236.
(3) Hollenstein, H.; Günthard, Hs. H. *Chem. Phys.* **1974**, *4*, 368−389.
(4) Amatatsu, Y.; Hamada, Y.; Tsuboi, M.; Sugie, M. *J. Mol. Spectrosc.* **1985**, *111*, 29−41.
(5) Sugie, M.; Takeo, H.; Matsumura, C. *Chem. Phys. Lett.* **1985**, *113*, 140−144.

S0002-7863(96)01063-3 CCC: $14.00 © 1997 American Chemical Society

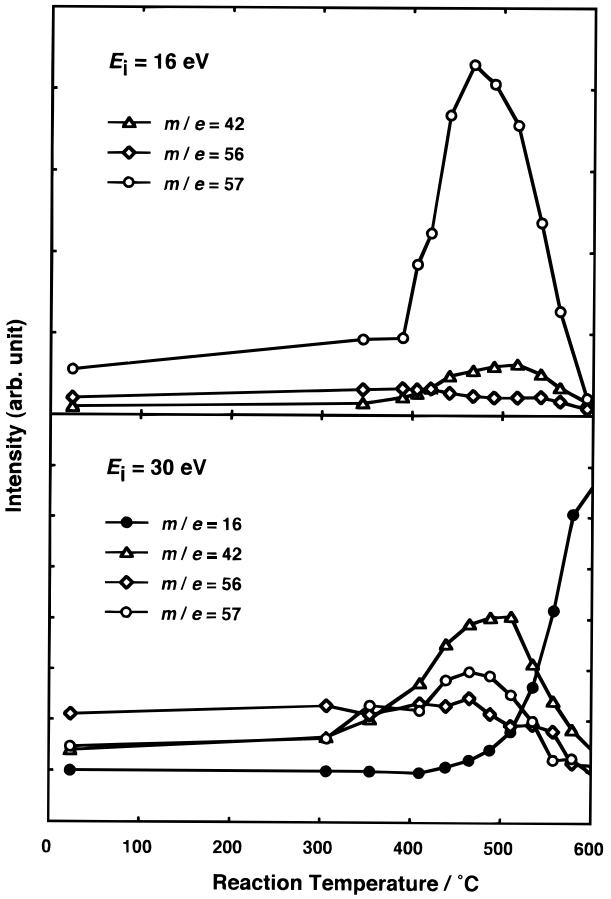

Figure 2. Mass spectral intensities vs the reaction temperature for E_i = 16 and 30 eV.

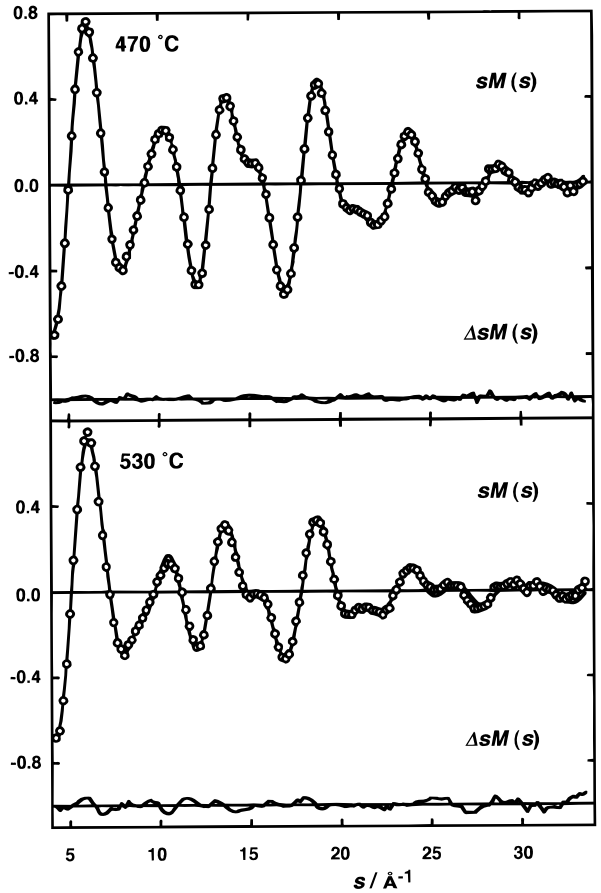

Figure 3. Experimental (○) and best-fit (—) molecular scattering intensities of pyrolysis products of propylenimine at the reaction temperatures of 470 and 530 °C; $\Delta sM(s) = sM(s)^{obs} - sM(s)^{calc}$.

NMEI.[5] They also observed some transitions which seemed to be of another unstable species, but they did not attribute them to *anti*-NMVA.

The reaction path for the pyrolysis of PI was also investigated theoretically by Sugie et al. by using HF/4-31G* basis set.[6] Again it was found that PI does not turn into *trans*-NMEI directly but first turns into *syn*-NMVA and then into *anti*-NMVA, which finally turns into *trans*-NMEI. It should be noted that the *anti* conformer of NMVA, which has not been identified explicitly in the spectra, plays an important role as an intermediate species.

The purpose of the present study was to apply the method of gas electron diffraction to this reaction system in order to determine the geometrical structures of these unstable species and to give a quantitative estimation of their amount. The authors have reported the electron diffraction study of thermal decomposition products of trimethylamine,[7] in which the geometrical structure of unstable *N*-methylmethylenimine ($CH_3-N=CH_2$) was determined. It was shown that this method was effective for not only the structural determination but also the identification and quantitative analysis of unstable species . Similarly to the previous study,[7] the results of *ab initio* calculations were utilized to assist the analyses in the present study. It seemed possible that precursor molecules, PI, remain in certain amount in the pyrolysis products and hence the analysis of the mixture of PI and unstable species would be necessary. Therefore, the geometrical structure of PI has already been determined by gas electron diffraction and reported elsewhere.[8]

Experimental Section

The sample of PI was purchased from Tokyo Chemical Industry Co., Ltd., and used without vacuum distillation because it was stabilized by NaOH. The details of the pyrolysis nozzle system are described in ref 7. In short, the sample gas is effused into the diffraction chamber through a nozzle tip immediately after it is heated in a spiral quartz tube. It should be noted that the reaction temperature is defined as that of the quartz tube, while the nozzle tip is nearly at room temperature (24 °C).

Prior to the electron diffraction experiment, the mass spectra of reaction products were measured by using a quadruple mass spectrometer (ULVAC, MSQ-400) attached to the electron diffraction apparatus[9] in order to determine the optimum reaction temperature. Figure 2 shows the temperature dependence of several peaks appearing in the mass spectra measured at the ionization electron energies (E_i) of 16 and 30 eV. In the spectrum for E_i = 16 eV, only the precursor molecule (PI, m/e = 57) could be detected. On the other hand, the peaks of m/e = 16, 42, and 56 were detected in the spectrum for E_i = 30 eV. The peak of m/e = 42 corresponds to the fragment ion which was created by demethylation of the m/e = 57 species in the ionization chamber, for the intensity ratio of m/e = 42 and 57 peaks is almost independent of the temperature but strongly dependent on the ionization electron energy. By increasing the temperature, the intensity of the peak of m/e = 57 began to increase at about 400 °C. This indicates the formation of the thermal rearrangement product which has a different ionization potential from that of PI. The peak intensity reached its maximum at about 470 °C, where the peak of m/e = 16 (CH_4^+) began to increase. These features show that the thermal rearrangement reaction of PI occurs at about 400−470 °C and the thermal decomposi-

(6) Sugie, M.; Aoyagi, M.; Takeo, H.; Matsumura, C. Symposium on Molecular Structure, Fukuoka, 1990.

(7) Fujiwara, H.; Egawa, T.; Konaka, S. *J. Mol. Struct.* **1995**, *344*, 217−226.

(8) Fujiwara, H.; Egawa, T.; Takeuchi, H.; Konaka, S. *J. Mol. Struct.* **1996**, *380*, 63−74.

(9) Konaka, S.; Kimura, M. Symposium on Gas Phase Molecular Structure, Austin, TX, 1990.

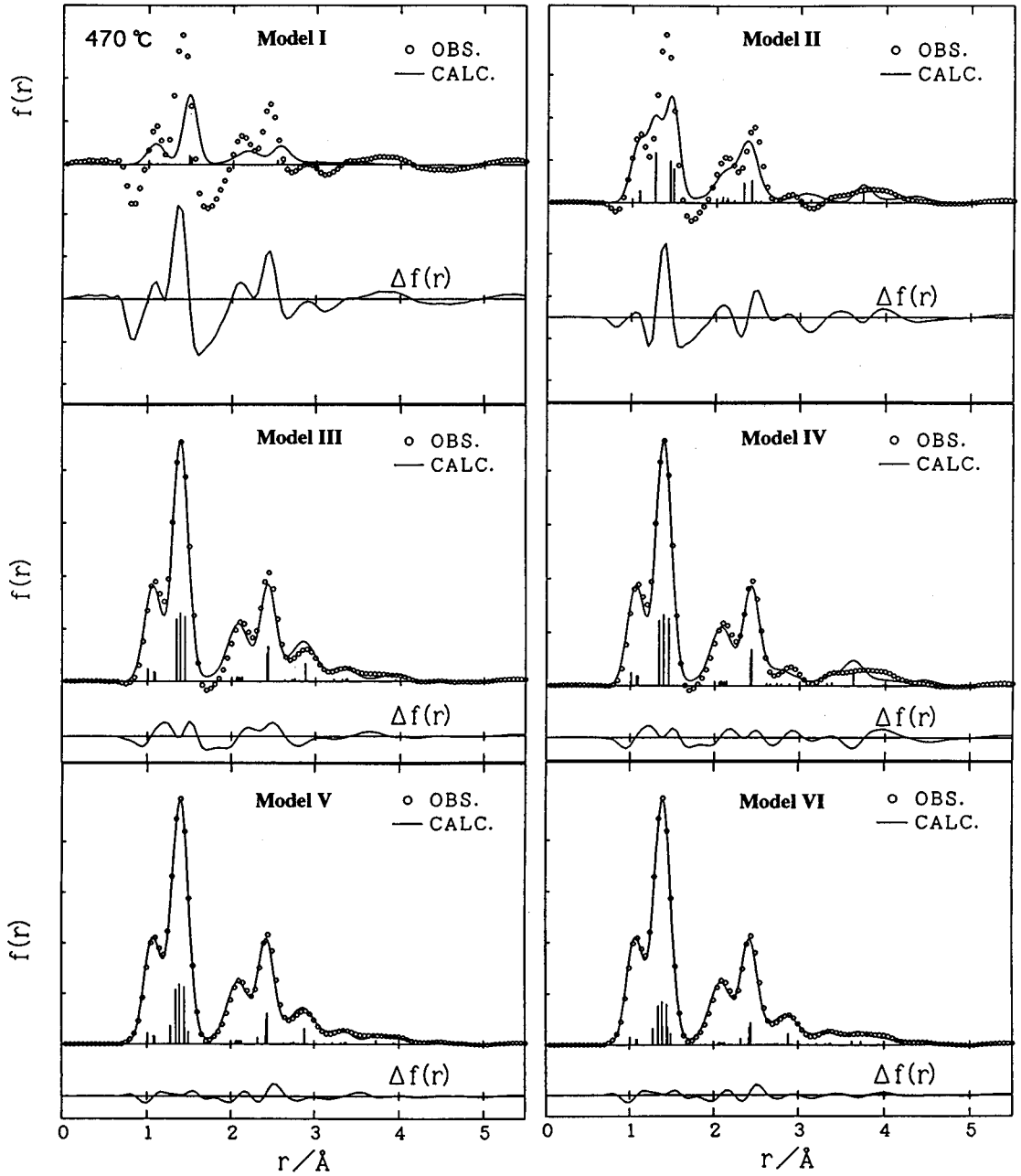

Figure 4. Experimental (○) and calculated (—) radial distribution curves for models I to VI at the reaction temperature of 470 °C; $\Delta f(r) = f(r)^{obs} - f(r)^{calc}$. Compositions for models are as follows: model I, *trans*-PI (69%) and *cis*-PI (31%); model II, *trans*-NMEI (100%); model III, *syn*-NMVA (100%); model IV, *anti*-NMVA (100%); model V, *syn*-NMVA(78%) and *trans*-NMEI (22%); model VI, *syn*-NMVA (56%), *anti*-NMVA (25%), and t*rans*-NMEI (19%).

tion reaction dominates at higher temperature. Considering these results, the reaction temperatures of 470 and 530 °C were chosen for the electron diffraction experiment in order to investigate both reactions of PI.

Electron diffraction patterns were recorded on 8 × 8 inch Kodak projector slide plates using an apparatus equipped with an r^3 sector.[9] The camera distance was 245.1 mm and the acceleration voltage was about 37 kV. The electron wavelength was calibrated with reference to the r_a (C═S) distance of CS_2 (1.5570 Å)[10] and determined to be 0.06364 Å. Other experimental conditions were as follows: uncertainty of scale factor, 0.04%; range of *s* value, 4.2−33.5 $Å^{-1}$; beam current, 2.8 μA; sample pressure, 25−30 Torr; background pressure, 7×10^{-6} Torr (470 °C) and $3.2-3.5 \times 10^{-5}$ Torr (530 °C); exposure time, 54 s.

Optical densities were measured with a microphotometer of a double-beam type at intervals of 0.1 mm along the diameter. Five adjacent points were averaged and converted to the total intensity. The total intensities thus obtained at intervals of 0.5 mm were averaged for three and two plates for 470 and 530 °C, respectively. They were divided by theoretical backgrounds and were used for data analysis. Elastic and inelastic scattering factors were taken from refs 11 and 12, respectively. Figure 3 shows the obtained molecular scattering intensities. The leveled total intensities and the backgrounds are listed in Table SI (Supporting Information).

Theoretical Calculations

Geometrical optimizations of *syn*-NMVA, *anti*-NMVA, and *trans*-NMEI were carried out with MP2 level[13] by using 6-31G** basis set[14] in advance of the analyses of the electron diffraction data. These species

(10) Tsuboyama, A.; Murayama, A.; Konaka, S.; Kimura, M. *J. Mol. Struct.* **1984**, *118*, 351−354.

(11) Kimura, M.; Konaka, S.; Ogasawara, M. *J. Chem. Phys.* **1967**, *46*, 2599−2603.

(12) Tavard, C.; Nicolas, D.; Rouault, M. *J. Chim. Phys. Phys.-Chim. Biol.* **1967**, *64*, 540−554.

(13) Møller, C.; Plesset, M. S. *Phys. Rev.* **1934**, *46*, 618−622.

are possible candidates for the thermal rearrangement products of PI.[6] Computer program GAUSSIAN 86 was used.[15] The resultant structural parameters and the energies of *syn*- and *anti*-NMVA are listed in Table SII, where it is shown that the *syn* conformer is more stable by about 1.2 kcal/mol. Table SII also lists the results of calculations for *trans*-NMEI.

Harmonic force constants in the Cartesian coordinates were also obtained for *syn*- and *anti*-NMVA by HF/6-31G** calculations. Computer program GAUSSIAN 92 was used.[16]

Analyses

Preliminary Analysis of the Electron Diffraction Data Taken at 470 °C. In order to predict the composition of products at 470 °C, a preliminary analysis of the electron diffraction data was carried out. The abundance of each conformer was treated as an adjustable parameter while the geometrical parameters were fixed at their experimental or theoretical values. The following six models were tested by comparison with the experimental data. Model I is the mixture of *trans*- and *cis*-PI with the abundance at room temperature reported in the literature,[8] which are 0.69 and 0.31 for the *trans* and *cis*, respectively. Models II, III, and IV consist of only *trans*-NMEI, *syn*-NMVA, and *anti*-NMVA, respectively. Model V is the mixture of *syn*-NMVA and *trans*-NMEI, and model VI is the mixture of *syn*- and *anti*-NMVA and *trans*-NMEI.

Figure 4 compares the resultant radial distribution (RD) curves for six models. The observed RD curve slightly depends on the model because the calculated $sM(s)$ for each model were used for $0 \le s \le 4.2$ Å^{-1}, in place of the observed one. In the case of model I (no pyrolysis model), discontinuity between the calculated $sM(s)$ for $s \le 4.2$ Å^{-1} and the observed $sM(s)$ for $s \ge 4.2$ Å^{-1} is so serious that the observed RD curve shows large negative background, and the obtained best-fit $sM(s)$ has extremely low index of resolution (0.20 ± 0.13). Therefore, this model can clearly be ruled out. It is also apparent that models II to IV (single species models) reproduce the observed RD quite unsatisfactorily. Next data analyses were performed on the basis of partially pyrolysis models, namely, the combinations of PI plus *trans*-NMEI, PI plus *syn*-NMVA, and PI plus *anti*-NMVA. However, the abundance of PI for each of these models was found to be zero within error limits; i.e., these models gave essentially the same results as in the case of models II to IV. Therefore, it is clear that at 470 °C, PI no longer remains and completely changes into some other species.

As shown in Figure 4, models V and VI, reasonably reproduce the observation. Model VI is slightly better than V. The resultant abundance of each species in model VI was found to be significant. Namely, it is 56 ± 20, 25 ± 22, and 19 ± 4% for *syn*-NMVA, *anti*-NMVA, and *trans*-NMEI, respectively. Therefore, all these rearrangement products were included in the following structural analysis.

Normal Coordinate Analysis. The force constants, F_x, of NMVA given by the HF/6-31G** calculations were converted into the force constants, F_{ij}, in internal coordinates. Then the F_{ij} of *syn*-NMVA were modified by a scale factor method,[17] in which scale factors were adjusted so that the vibrational frequencies observed by Amatatsu et al.[4] were reproduced. The resultant scale factors for the *syn* conformer were applied also for the *anti* conformer. The observed and calculated vibrational frequencies are listed in Table 1. The definitions of internal coordinates and the force constants thus obtained are listed in Table SIII.

As for *trans*-NMEI, Hollenstein and Günthard have measured its vibrational frequencies and determined the force constants.[3] However, the geometry used in their normal coordinate analysis had been estimated from the rotational constants under some assumptions,[2] and the values of some parameters are somewhat unreasonable. For example, the N═C distance, 1.30 Å, seems to be too long and the N−C distance, 1.43 Å, too short. In the present study, therefore, the geometry optimized by MP2/6-31G** calculations was adopted and the force constants of Hollenstein and Günthard were revised so as to reproduce the vibrational frequencies measured by them. The results are listed in Table SIV.

Mean amplitudes and shrinkage corrections, $r_\alpha - r_a$,[18] for these three species were calculated from the derived force constants. The results are listed in Table SV. These parameters are fixed at their calculated values throughout the following data analyses.

Analysis of Electron Diffraction Data Taken at the Reaction Temperature of 470 °C. As described in the Preliminary Analysis section, the electron diffraction data at the reaction temperature of 470 °C were analyzed by assuming that *syn*- and *anti*-NMVA and *trans*-NMEI were present. It is impractical to determine all the structural parameters of the three species independently. Therefore, the differences between the structural parameters of different species as well as the differences between some structural parameters of the same species were fixed at the corresponding values of MP2/6-31G** optimization. All the dihedral angles and all the bond angles including H atoms were fixed at the MP2/6-31G** values.

There are nine nonequivalent skeletal bond lengths, but they could not be determined independently. Therefore, the nine bond lengths were divided into three groups as follows. According to the MP2/6-31G** calculations, the N_1-C_2 single bond lengths for *syn*- and *anti*-NMVA are about 1.39 Å (Table SII). This value is significantly different from that of a normal N−C single bond and N═C double bond. Therefore, the N_1-C_2 bond lengths of *syn*- and *anti*-NMVA were adjusted as one group. The $r(N_1-C_3)$ for all the species and $r(C_2-C_4)$ of *trans*-NMEI were treated as another group. The third group consisted of double bonds, that is, the $r(C_2═C_4)$ of *syn*- and *anti*-NMVA and the r(N═C) of *trans*-NMEI. In addition to these skeletal bond lengths, all the C−H and N−H bond lengths were adjusted as one group.

The bond angles of skeletal atoms were divided into two groups as follows. The C−N−C angles of *syn*- and *anti*-NMVA and the C−N═C angle of *trans*-NMEI were adjusted as the first group. The N−C═C angles of *syn*- and *anti*-NMVA and the N═C−C angle of *trans*-NMEI were adjusted as the second group.

Table SVI summarizes adopted constraints. In addition to the six adjustable structural parameters of *syn*-NMVA, $r(N_1-C_2)$, $r(N_1-C_3)$, $r(C_2═C_4)$, $r(C_2-H_5)$, C−N−C angle, and N−C═C angle, the index of resolution and the abundances of

(14) Hariharan, P. C.; Pople, J. A. *Theor. Chim. Acta* **1973**, *28*, 213−222.

(15) Frisch, M. J.; Binkley, J. S.; Schlegel, H. B.; Raghavachari, K.; Melius, C. F.; Martin, R. L.; Stewart, J. J. P.; Bobrowicz, F. W.; Rohlfing, C. M.; Kahn, L. R.; DeFrees, D. J.; Seeger, R.; Whiteside, R. A.; Fox, D. J.; Fluder, E. M.; Topiol, S.; Pople, J. A. Carnegie-Mellon Quantum Chemistry Publishing Unit, Carnegie-Mellon University: Pittsburgh, PA, 1984.

(16) Frisch, M. J.; Trucks, G. W.; Head-Gordon, M.; Gill, P. M. W.; Wong, M. W.; Foresman, J. B.; Johnson, B. G.; Schlegel, H. B.; Robb, M. A.; Replogle, E. S.; Gomperts, R.; Andres, J. L.; Raghavachari, K.; Binkley, J. S.; Gonzalez, C.; Martin, R. L.; Fox, D. J.; DeFrees, D. J.; Baker, J.; Stewart, J. J. P.; Pople, J. A. Gaussian, Inc.: Pittsburgh, PA, 1992.

(17) Boggs, J. E. In *Stereochemical Applications of Gas-Phase Electron Diffraction, Part B*; Hargittai, I., Hargittai, M., Eds.; VCH Publishers, Inc.: New York, 1988; Chapter 10.

(18) Kuchitsu, K.; Cyvin, S. J. In *Molecular Structures and Vibrations*; Cyvin, S. J., Ed.; Elsevier: Amsterdam, 1972; Chapter 12.

Table 1. Observed and Calculated Vibrational Frequencies (in cm^{-1}) and Assignments for *N*-Methylvinylamine

	syn-NMVA		*anti*-NMVA	
ν_{obs}[a]	ν_{calc}	PED (%)[b]	ν_{calc}	PED (%)[b]
3485	3483	S_4 (100)		
			3452	S_4 (100)
3120	3097	S_1 (99)	3088	S_1 (93)
3037	3027	S_2 (51), S_3 (47)	3018	S_3 (90)
2990	3014	S_3 (52), S_2 (48)	3000	S_2 (88)
2928	2922	S_6 (88)	2919	S_6 (85)
2868	2886	S_{19} (68), S_5 (26)	2883	S_{19} (64), S_5 (28)
2822	2810	S_5 (73), S_{19} (22)	2807	S_5 (72), S_{19} (23)
1655	1657	S_7 (62), S_{16} (19), S_{12} (17)	1668	S_7 (58), S_{16} (18), S_8 (15)
1495	1495	S_{15} (66), S_8 (19)	1487	S_{12} (43), S_{15} (36)
1465	1456	S_{11} (48), S_{12} (32)		
1445	1442	S_{11} (42), S_{12} (37)	1451	S_{11} (60), S_{20} (27)
1430	1427	S_{20} (93)	1432	S_{20} (54), S_{11} (27), S_{10} (17)
1405	1392	S_{10} (92)	1411	S_{10} (61)
			1377	S_{15} (30), S_{10} (27), S_{12} (20)
1315	1314	S_{16} (52), S_7 (18)	1303	S_{16} (51), S_7 (22)
			1262	S_8 (37)
1230	1226	S_9 (25), S_8 (16)		
1150	1135	S_{14} (58)	1151	S_9 (64)
			1106	S_{21} (51), S_{14} (39)
1063	1092	S_{21} (82)		
1029	1034	S_{13} (44), S_9 (38)	1026	S_{13} (27), S_{21} (25), S_{14} (22)
966	973	S_{24} (55), S_{25} (46)	978	S_{24} (53), S_{25} (46)
920	917	S_8 (34), S_9 (19)	896	S_{13} (38), S_8 (26), S_9 (16)
795	795	S_{23} (102)	800	S_{23} (100)
			723	S_{22} (47), S_{24} (21)
661	656	S_{25} (45), S_{24} (40)	637	S_{25} (41), S_{24} (19), S_{18} (16)
527	612	S_{18} (51), S_{17} (27), S_{22} (18), S_{13} (17)		
408	495	S_{22} (75), S_{17} (35), S_{26} (16)	483	S_{17} (53)
	284	S_{18} (26), S_{27} (19), S_{17} (18), S_{22} (17)	307	S_{18} (53), S_{17} (32)
	252	S_{26} (71), S_{27} (41)		
	229	S_{27} (46), S_{26} (21)	208	S_{27} (94)
			127	S_{26} (88), S_{22} (40),

[a] The fundamental frequencies observed by Amatatsu et al.[4] [b] Potential energy distribution for the local symmetry coordinates S_i given in Table SIIIa. Contributions less than 15% are not shown. The characters of S_i are as follows: S_1, CH_2 a-str; S_2, CH_2 s-str; S_3, C−H str; S_4, N−H str; S_5, CH_3 s-str; S_6, CH_3 a-str; S_7, C═C str; S_8, N−C_2 str; S_9, N−C_3 str; S_{10}, CH_3 s-def; S_{11}, CH_3 a-def; S_{12}, CH_2 sciss; S_{13}, CH_2 rock; S_{14}, CH_3 a-rock; S_{15}, CNH a-bend; S_{16}, CCH bend; S_{17}, NCC bend; S_{18}, CNC bend; S_{19}, CH_3 a-str; S_{20}, CH_3 a-def; S_{21}, CH_3 a-rock; S_{22}, CNH s-bend; S_{23}, CH_2 wag; S_{24}, C−H out of plane; S_{25}, C═C torsion; S_{26}, N−C_2 torsion; S_{27}, N−C_3 torsion, where s and a denote sym and asym, respectively.

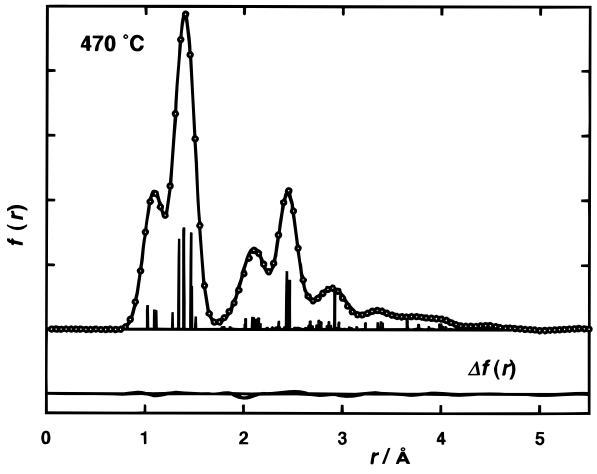

Figure 5. Experimental (○) and calculated (—) radial distribution curves for the final analysis of data at the reaction temperature of 470 °C. The theoretical curve is for the *syn*-NMVA (63%) + *anti*-NMVA (28%) + *trans*-NMEI (9%) mixture. $\Delta f(r) = f(r)^{obs} - f(r)^{calc}$.

the two species were determined by least-squares calculations on the molecular scattering intensities. The abundance of the third species is not independent. Figure 5 shows resultant RD curves and the results of the analysis are listed in Table 2.

Analysis of Electron Diffraction Data Taken at the Reaction Temperature of 530 °C. The data taken at 530 °C were analyzed by fixing all the structural parameters similarly to the preliminary analysis of the data at 470 °C. Only the abundance and the index of resolution were adjusted. The following three models were tested. Model I is the mixture of *syn*- and *anti*-NMVA and *trans*-NMEI, namely, the same species as detected in the 470 °C experiment. Their structural parameters were fixed at the values determined by the analysis of the 470 °C data. In model II, methane and acetonitrile were added to model I. These two species are possible pyrolysis products of *trans*-NMEI. The structural parameters of methane were

Table 2. Thermal Average Structures of *N*-Methylvinylamine and *trans*-*N*-Methylethylidenimine (r_g in Å and $\angle_\alpha$ in deg) and Mole Fractions at Reaction Temperature 470 °C[a]

	syn-NMVA	*anti*-NMVA	*trans*-NMEI	
r(N−C_2)	1.391(3)	1.395(3)	r(N═C)	1.278(4)
r(N−C_3)	1.465(3)	1.472(3)	r(N−C)	1.472 } (3)
r(C═C)	1.343(4)	1.341(4)	r(C−C)	1.511 } (3)
r(C−H_5)	1.105 } (2)	1.106 } (2)	r(C−H_5)	1.119(2)
r(N−H)	1.029 } (2)	1.033 } (2)		
∠CNC	119.5(9)	118.4(9)	∠CNC	118.0(9)
∠NCC	126.5(7)	126.1(7)	∠NCC	121.4(7)
ϕ(CNCC)[b]	13.1	−145.1		180.0
mole fraction	0.63(7)	0.28(8)		0.09(4)
k[c]	0.88(1)	R[d]	0.043	

[a] Structural parameters at 24 °C. Values in parentheses are 3σ. See Figure 1 for the atom numbering. [b] Fixed to the values of MP2/6-31G** ab initio calculations. [c] Index of resolution. [d] $R = \{\sum_i W_i(sM(s)_i^{obs} - sM(s)_i^{calc})^2/\sum_i W_i(sM(s)_i^{obs})^2\}^{1/2}$, where W_i is a diagonal element of the weight matrix.

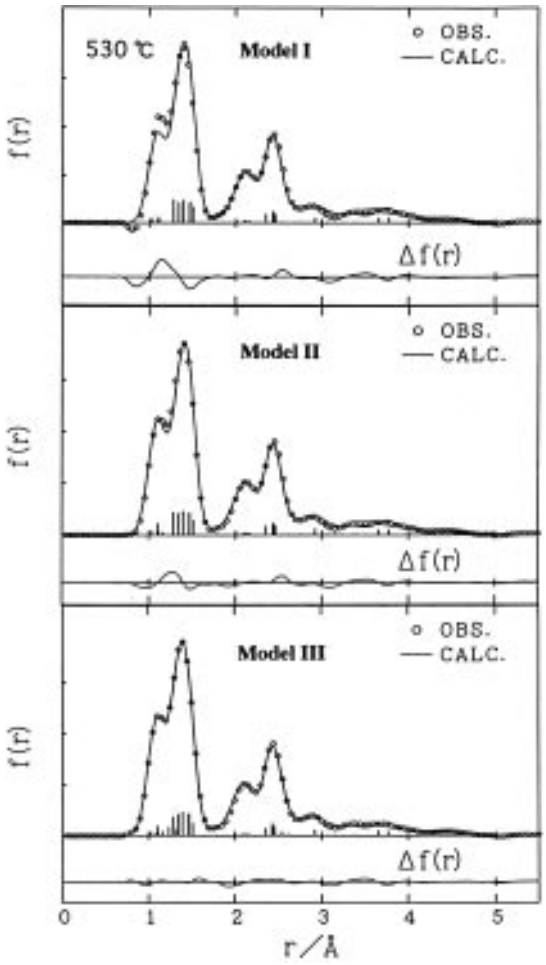

Figure 6. Experimental (○) and calculated (—) radial distribution curves for models I to III at the reaction temperature of 530 °C; $\Delta f(r) = f(r)^{obs} - f(r)^{calc}$. Compositions for models are as follows: model I, *syn*-NMVA (32%), *anti*-NMVA (36%), and *trans*-NMEI (32%); model II, *syn*-NMVA (27%), *anti*-NMVA (26%), *trans*-NMEI (22%), CH_4 (23%), and CH_3CN (2%); model III, *syn*-NMVA (25%), *anti*-NMVA (26%), *trans*-NMEI (18%), CH_4 (19%), CH_3CN (4%), and CH_2═C═NH (8%).

fixed at the values determined by electron diffraction,[19] and those of acetonitrile were taken from the values determined by a joint analysis of electron diffraction data and rotational constants.[20] In addition, in model III, ketenimine (KI, CH_2═C═NH) was added to model II, for NMVA is expected to decompose into KI and methane. KI is an unstable species and no experimental geometry is available. Therefore, we used the theoretical one determined by Brown et al. from the MP3/6-31G** calculations.[21] The harmonic force constants of KI were determined by modifying the theoretical values given by HF/6-31G** calculations[21] so as to reproduce the vibrational frequencies measured in the Ar matrix.[22] The force constants thus obtained were used to calculate the mean amplitudes and shrinkage corrections of KI.

Figure 6 shows RD curves for models I to III. The existence of the same species as those for the 470 °C experiment was assumed in model I. In this model, large residuals remained from 0.7 to 1.6 Å but residuals were only slight for $r > 3$ Å. Therefore, there probably exist some decomposition products

(19) Bartell, L. S.; Kuchitsu, K.; deNeui, R. J. *J. Chem. Phys.* **1961**, *35*, 1211−1218.
(20) Karakida, K.; Fukuyama, T.; Kuchitsu, K. *Bull. Chem. Soc. Jpn.* **1974**, *47*, 299−304.
(21) Brown, R. D.; Rice, E. H. N.; Rodler, M. *Chem. Phys.* **1985**, *99*, 347−356.

Table 3. Rotational Constants of *syn*-*N*-Methylvinylamine and *trans*-*N*-Methylethylidenimine (in GHz)[a]

	B_0 (MW)[b]	B_z(MW)[c]	B_α^0(ED)[d]
	syn-*N*-Methylvinylamine		
A	17.413011(14)[e]	17.431(4)	17.39(9)
B	5.974342(4)[e]	5.9698(11)	5.94(3)
C	4.586645(4)[e]	4.5857(2)	4.579(14)
	trans-*N*-Methylethylidenimine		
A	38.35863(14)[f]	38.57(7)	38.46(16)
B	4.078135(17)[f]	4.07807(2)	4.031(12)
C	3.86274(2)[f]	3.86237(9)	3.819(10)

[a] Values in parentheses are error limits. [b] Observed rotational constants. [c] Derived from B_0 by making vibrational corrections. The error limits were estimated to be $0.24|B_0 - B_z|$. [d] Calculated from the r_α^0 structure determined from electron diffraction data. The definitions of r_α^0 and r_z are the same.[23] The error limits were estimated to be 3σ. [e] Reference 5. [f] Reference 2.

of NMVA and/or *trans*-NMEI, and there seems to be no polymerized product. In the mass spectra, the peak of m/e = 16 increased rapidly over 470 °C as shown in Figure 2. Thus, it is clear that methane exists in this temperature region. The addition of methane and acetonitrile to model I, i.e., model II, improved fitting quality significantly. However, significant residuals still remained between 1.1 and 1.4 Å in model II. Finally, satisfactory agreement of observed and calculated RD curves was obtained by adding KI to model II (model III). The residuals appearing from 1.1 to 1.4 Å in model II can be attributed to the N═C and C═C double bonds of KI, and slighter residuals around 2.5 Å are ascribable to the nonbonded N···C atomic pair. The determined abundance of each species is as follows: *syn*-NMVA, 25 ± 10%; *anti*-NMVA, 26 ± 10%; *trans*-NMEI, 18 ± 2%; methane, 19 ± 4%; acetonitrile, 4 ± 2%; KI, 8 ± 2%.

Results and Discussion

Geometrical Structures. Table 2 lists the experimentally determined geometrical structures of *syn*- and *anti*-NMVA and *trans*-NMEI (r_g and $\angle_\alpha$). The r_α structures obtained in the present study were extrapolated to the zero-point average structures (r_α^0),[18] from which the rotational constants (A_α^0, B_α^0, and C_α^0) were calculated. On the other hand, the observed rotational constants, A_0, B_0, and C_0, of *syn*- NMVA[5] and *trans*-NMEI[2] were converted to A_z, B_z, and C_z by applying vibrational corrections.[18] As listed in Table 3, the rotational constants of *syn*-NMVA are reproduced within errors, which shows the accuracy of the geometrical structure obtained in the present study. On the other hand, there is slight but significant discrepancy for the *B* and *C* constants of *trans*-NMEI. This can be attributed to the fact that the structure of *trans*-NMEI is determined rather indirectly from that of NMVA and the constraints because of its low abundance (9 ± 4%). Therefore, the error limits for the structural parameters of *trans*-NMEI should be larger than those listed in Tables 2 and 4. The error estimation for *anti*-NMVA should be somewhat optimistic for the same reason. At the present stage, however, more precise error estimation is difficult for *anti*-NMVA and *trans*-NMEI.

The observed structures of these chemical species are compared with the corresponding r_e structures given by MP2/6-31G** calculations (Table SII). The calculated lengths of the N−C_2 single bonds of NMVA (1.389 and 1.393 Å for *syn*

(22) Jacox, M. E. *Chem. Phys.* **1979**, *43*, 157−172.

Table 4. Comparison of r(N═C) (in Å)[a]

	trans-CH_3−N═CH−CH_3	CH_3−N═CH_2	HN═CH_2
observed	1.278(4)[b]	1.281(6)[c]	1.273(4)[d]
HF/6-31G**	1.2484[e]	1.246[f]	1.2500[g]
MP2/6-31G**	1.2785[e]	1.2765[g]	1.2800[h]
MP3/6-31G**			1.274[i]
MP4/6-31G**			1.2848[h]

[a] Values in parentheses are error limits. [b] r_g distance, this work. [c] r_g distance, ref 7. [d] r_s distance, ref 23. [e] This work. [f] Reference 24. [g] Reference 7. [h] Reference 25. [i] Reference 26.

and *anti*, respectively), the C═C double bonds of NMVA (1.343 and 1.341 Å for *syn* and *anti*, respectively), and the N═C double bond of *trans*-NMEI (1.278_5 Å) are in reasonable agreements with the experimental ones. On the other hand, the experimental values are about 0.02 Å longer than the calculated ones for r(N−C_3) of all species (1.447, 1.454, and 1.453 Å for *syn*-NMVA, *anti*-NMVA, and *trans*-NMEI, respectively) and r(C−C) of *trans*-NMEI (1.493 Å), which belong to the same group of adjustable parameters in the data analysis. This discrepancy is beyond the difference of the physical meanings of r_g and r_e. The NCC angle of each species agrees with the calculated one, 126.6°, 126.3°, and 121.5° for *syn*-NMVA, *anti*-NMVA, and *trans*-NMEI, respectively. However, there is a discrepancy of about 1.5° for the CNC angle of each species, which exceeds the experimental error, since the calculated CNC angles are 118.0°, 116.9°, and 116.5° for *syn*-NMVA, *anti*-NMVA, and *trans*-NMEI, respectively.

Only a limited number of N═C bond lengths are available for small molecules because of molecular unstability. Table 4 compares the N═C distance of *trans*-NMEI with those of related molecules and their theoretical values. Here, the structure of *trans*-NMEI was optimized at the HF level by using the 6-31G** basis set for comparison. There is no significant difference between the observed N═C distances of *trans*-NMEI and *N*-methylmethylenimine.[7] In addition, the N═C distance of methylenimine (H−N═CH_2)[23] is in moderate agreement with them if we take account of the difference between r_g and r_s distances. The theoretical values of r(N═C) calculated at HF level are shorter than the experimental values by 0.023−0.035 Å. Thus it is concluded that calculation at MP2 or better level is necessary to reproduce the experimental N═C bond length.

Reaction Path. Sugie et al. assumed two reaction paths for the thermal rearrangement of PI into *trans*-NMEI and investigated their possibilities by HF/4-31G* *ab initio* calculations.[6] In path I, PI directly turns into *trans*-NMEI through some transition states but through no intermediate species. In path II, however, PI first turns into *syn*-NMVA and then into *anti*-NMVA, which finally turns into *trans*-NMEI (see Figure 7). They found that the energy of the transition state on path I (TS3 in Figure 7) is higher than those on path II (TS2 and TS4), and, hence, they concluded that the latter path is more plausible. This is consistent with the time evolution of the IR spectrum reported by Amatatsu et al.[4]

In the present study, the abundance of *syn*-NMVA decreased from 63 to 25% by increasing the reaction temperature from 470 to 530 °C, while that of *trans*-NMEI increased from 9 to

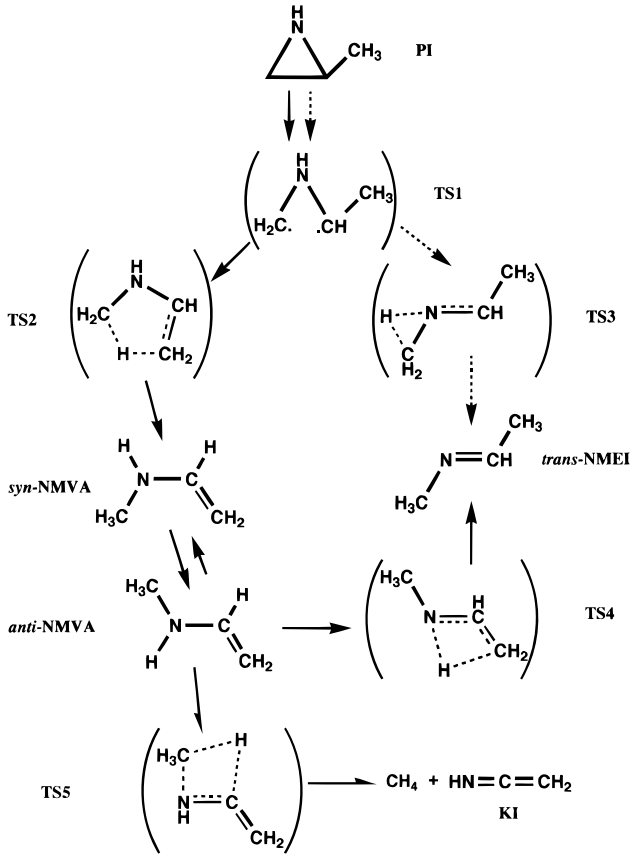

Figure 7. Possible pyrolysis reaction paths of propylenimine. Transition states are labeled as TS. Dashed arrows indicate path I and solid arrows indicate path II (see Results and Discussion). Half arrows indicate decomposition of *anti*-NMVA.

18%. The increasing abundance of *trans*-NMEI with increasing reaction temperature indicates that *trans*-NMEI is not directly formed from PI. This is in agreement with the reaction path suggested by previous experimental and theoretical studies as mentioned above.[4,6] It should be noted that the existence of *anti*-NMVA in the pyrolysis products was experimentally found for the first time in the present study. At the reaction temperatures of 470 and 530 °C, the abundance of *anti*-NMVA was found to be significant; that is, it was 28 ± 8% and 26 ± 10% for 470 °C and 530 °C, respectively. In contrast with the results of the IR spectroscopic study,[4] all three unstable species, *syn*- and *anti*-NMVA and *trans*-NMEI, were found to coexist in the present experimental condition.

This difference can be attributed to the difference in the flow condition. In the present experiment, a hypodermic needle with an i.d. of 0.5 mm was used for the needle tip, which might cause the stagnation of the gas flow before the outlet and hence it might be possible for some portion of *syn*-NMVA to change into *anti*-NMVA and *trans*-NMEI in the quartz tube. According to MP2/6-31G** calculations, the energy of NMEI is lower than that of *syn*-NMVA by about 8.8 kcal mol^{-1} (Table SII). Therefore, the small abundance of *trans*-NMEI shows that it comes out from the nozzle before the reactions reach thermal equilibrium. In the measurement of the IR spectrum,[4] however, the pyrolysis products (mostly NMVA) were introduced into the cell which was kept at room temperature, and thus it took longer for NMVA to change into NMEI than in the present study. In the microwave spectroscopic study,[5] the existence of *anti*-NMVA is not clear because Sugie et al. reported the spectral lines of an unidentified unstable species in addition to those of

(23) Callomon, J. H.; Hirota, E.; Iijima, T.; Kuchitsu, K.; Lafferty, W. J. *Landolt-Börnstein, New Series*; Springer-Verlag: Berlin, 1987; Vol. II/15.

(24) Armstrong, D. R.; Walker, G. T. *THEOCHEM* **1987**, *149*, 369−389.

(25) Panchenko, Y. N.; De Maré, G. R.; Bock, C. W. *J. Mol. Struct.* **1992**, *272*, 161−177.

(26) Rodler, M.; Brown, R. D.; Godfrey, P. D.; Kleibömer, B. *J. Mol. Spectrosc.* **1986**, *118*, 267−276.

syn-NMVA and *trans*-NMEI. The unknown chemical species makes it difficult to discuss the difference between the experimental conditions of the present electron diffraction and the microwave spectroscopy.[5]

At the reaction temperature of 530 °C, the mole fractions of several chemical species were determined and we should be careful in discussing the pyrolysis products with small abundances. It is, however, reasonable to explain the formation of KI by the elimination of methane from NMVA. If we compare the geometries of its *syn* and *anti* isomers, *anti*-NMVA seems to be the precursor of KI and methane (see Figure 7).

Acknowledgment. The authors thank the Computer Center of the Institute for Molecular Science, Okazaki National Research Institutes, for the use of computers NEC SX-3/34R and Hitac S820, and library programs GAUSSIAN 86 and GAUSSIAN 92. Numerical computations were carried out on the Hitac M-682H and M-880 at the Hokkaido University Computing Center.

Supporting Information Available: The leveled total intensities and the backgrounds (Table SI), the results of MP2/6-31G** ab initio calculations (Table SII), the symmetry coordinates and the harmonic force constants of *syn*- and *anti*-*N*-methylvinylamine (Table SIII), the symmetry coordinates, the harmonic force constants and the observed and calculated vibrational frequencies of *N*-methylethylidenimine (Table SIV), the mean amplitudes and shrinkage corrections of *N*-methylvinylamine and *N*-methylethylidenimine except nonbonded H···H pairs (Table SV), structural constraints (Table SVI), and the correlation matrices (Table SVII) (30 pages). See any current masthead page for ordering and Internet access instructions.

JA961063D